Applied Catalysis B: Environmental 182 (2016) 369–374

Contents lists available at ScienceDirect

Applied Catalysis B: Environmental

journal homepage: www.elsevier.com/locate/apcatb

Highly functional titania nanoparticles produced by flame spray pyrolysis. Photoelectrochemical and solar cell applications

Iosif Tantis[a], Maria Vittoria Dozzi[b], Luca Giacomo Bettini[c,d], Gian Luca Chiarello[b], Vassilios Dracopoulos[e], Elena Selli[b,c,**], Panagiotis Lianos[a,e,*]

[a] Department of Chemical Engineering, University of Patras, 26500 Patras, Greece
[b] Department of Chemistry, University of Milan, Via Golgi 19, I-20133 Milano, Italy
[c] CIMAINA, University of Milan, Via Celoria 16, I-20133 Milano, Italy
[d] Department of Physics, University of Milan, Via Celoria 16, I-20133 Milano, Italy
[e] FORTH/ICE-HT, P.O. Box 1414, 26504 Patras, Greece

ARTICLE INFO

Article history:
Received 23 June 2015
Received in revised form
11 September 2015
Accepted 18 September 2015
Available online 21 September 2015

Keywords:
Flame spray pyrolysis
Titania
Photoelectrochemical cells

ABSTRACT

Nanoparticulate titania was synthesized by flame spray pyrolysis and was used to construct photoanodes for photoelectrochemical cells and quantum dot sensitized solar cells. Powders obtained by flame spray pyrolysis were composed of smaller nanoparticles and had higher specific surface areas than common commercial types of titania and this was carried over to the structure of the photoanodes and reflected on the photoelectrocatalytic and solar cell behavior of the photoanodes. The highest specific surface area and the smallest nanoparticle size produced in this work were 249 $m^2 g^{-1}$ and 7 nm, respectively. CdS-sensitized photoanodes were affected by the amount of the deposited sensitizer, which was the largest in the case of the powder with the highest specific surface area. When, however, the photoanodes were loaded with a relatively large amount of CdSe sensitizer, the role of the latter increased and the differences between the different forms of titania diminished.

1. Introduction

Nanoparticle titania is the best photocatalyst, for very good reasons. It is easily synthesized and manipulated, it is stable, it easily oxidizes water, thanks to its highly positive valence band potential (about 3 V *vs* SHE) and it is applicable to all photocatalytic and photoelectrocatalytic processes. Many attempts have been made to synthesize titania in several types of familiar and exotic forms and shapes, but it is a matter of fact that the best performances have been recorded with titania nanoparticles in the whole spectrum of its applications, starting from photocatalytic degradation of organic pollutants and ending up to perovskite solar cells [1–7]. It is then essential to search for easy, inexpensive and effective procedures of nanoparticle titania synthesis that will lead to massive production protocols of the best possible photoactive material. It is understood that the adjective "best" should be related with the efficacy of the nanoparticles and this quality is expected to be determined by the size, crystallinity and specific surface area of the nanoparticles.

With this in mind, in the present work we have studied titania produced by flame spray pyrolysis (FSP), a method that seems to be particularly fitted to the purpose of producing high quality titania nanoparticles as well as fluorinated [8] and noble-metal containing nanoparticles [9–12] for hydrogen production. Three FSP-made titania samples produced by specific protocols [13] were presently applied to photoelectrochemical cells and their performance was compared to that of the very well known commercial P25 titania. The purpose was not only to show the merits of such nanoparticle materials and to promote FSP as a particularly effective method of nanoparticle titania fabrication, but also to identify its limitations, so that dealing with these materials will be done in realistic terms. Even though, application of such photoactive materials may be envisaged in many different types of photoelectrochemical cells, we have chosen two types of representative cells, namely PhotoFuelCells including water oxidation [5,14] and quantum dot sensitized solar cells [15,16].

2. Experimental

2.1. Materials

Unless otherwise indicated, reagents were obtained from Aldrich and were used as received. The SnO_2:F used to produce

* Corresponding author at: Department of Chemical Engineering, University of Patras, 26500 Patras, Greece.
** Corresponding author at: Department of Chemistry, University of Milan, Via Golgi 19, I-20133 Milano, Italy.
E-mail addresses: elena.selli@unimi.it (E. Selli), lianos@upatras.gr (P. Lianos).

http://dx.doi.org/10.1016/j.apcatb.2015.09.040
0926-3373/

transparent conductive electrodes (FTO, Resistance 8 Ω/square) was purchased from Pilkington.

2.2. Synthesis of titania powders by flame spray pyrolysis

Titanium dioxide nanostructured powders with different structural properties and photocatalytic performance were synthesized by flame spray pyrolysis (FSP) starting from xylene solutions containing titanium(IV) isopropoxide (TTIP) as Ti precursor, employing the previously described commercial FSP burner system (NPS10, Tethis SpA, Italy) and procedure [13]. The powders were collected on a glass microfiber filter supported on a stainless steel filter, located downstream the FSP burner.

The synthesis parameters are listed in Table 1. In the present work, we focused attention on three distinct titania powders with broadly varying nanoparticle sizes and specific surface area (SSA), which were labeled FSPa, FSPb and FSPc. As shown in Table 1, FSPb was the powder with the smallest nanoparticle size and the largest SSA and FSPa the powder with the largest nanoparticles and the smallest SSA.

2.3. Preparation of titania films

Nanoparticle titania films were deposited on FTO transparent electrodes by the following procedure. A FTO glass was cut in the appropriate size and carefully cleaned first with soap and then by sonication in isopropanol, water and acetone. A thin layer of compact titania was first deposited over a patterned area by spraying a solution of 0.2 mol L^{-1} of diisopropoxytitanium bis(acetylacetonate) in ethanol and then calcine at 500 °C. Deposition of this bottom compact layer is a common practice in the fabrication of nanocrystalline titania photoanodes, since it enhances the adhesion of the top thick film, prevents short circuits and facilitates electron flow towards the electrode. On the top of this compact film, a titania paste made of FSP powders was applied, by doctor blading. The paste was obtained by mixing 100 mg of each FSP-made powder with 1.5 mL of ethanol, followed by sonication for about 3 h. The films were calcined up to 550 °C, with a heating rate of 20 °C min^{-1}. The thickness of the films was approximately 10 μm, as determined by their SEM profiles. The amount of titania was *ca.* 3 mg cm^{-2} in all films. The geometrical area of the films was 1 cm^2 (1 cm × 1 cm). For comparison, films were also made using Degussa P25 powder, under the same conditions employed to make the FSP-powder films. Particular care was taken to deposit approximately the same amount of photocatalyst in each film.

2.4. Deposition of CdS and CdSe sensitizers

When necessary, CdS was deposited on the TiO_2 films by 10 SILAR (Successive Ionic Layer Adsorption and Reaction) cycles, as previously described [17,18], using $Cd(NO_3)_2$ as Cd^{2+} and Na_2S as S^{2-} precursor, respectively, dissolved in water. The cation and anion concentration of the two aqueous solutions was 0.1 mol L^{-1}. After SILAR deposition and final washing with triply distilled water, the films were dried in an oven at 100 °C and were ready for use.

Some CdS/TiO_2/FTO photoanodes were further sensitized by CdSe. The latter was deposited from a chemical bath containing the Se and Cd precursors, according to the previously detailed standard procedure [15,19,20].

2.5. Preparation of the counter electrode

Two types of counter electrode were employed. In the case of photoelectrochemical cells for water oxidation and PhotoFuelCell applications, the counter electrode was a Pt foil. The active area exposed to the electrolyte solution was 1.5 cm × 1.5 cm. In the case of quantum dot sensitized solar cells, the counter electrode was a brass foil on which a Cu_2S layer was chemically grown, as previously described [15]. Its active area was also 1.5 cm × 1.5 cm.

2.6. Reactor

All current–voltage measurements were performed using a Plexiglas reactor, supporting on one side the photoanode electrode, which played the role of reactor window, and the counter electrode on the other side. As already mentioned, the active area of the photoanode was 1 cm^2, that of the cathode was 2.25 cm^2. The distance between the two electrodes was 5 mm. An Ag/AgCl reference electrode could be also accommodated in the reactor when necessary. The photoanode was illuminated by means of an Oriel LCS-100 solar simulator providing 100 mW cm^{-2} radiation. The reactor was filled with an aqueous solution, the composition of which depended on the particular application. In the case of water oxidation and PhotoFuelCell applications the solution contained 0.5 M NaOH, with or without 5% v/v ethanol; in the case of quantum dot sensitized solar cells a polysulfide solution was employed, containing 1.0 M Na_2S and 1.0 M sulfur.

2.7. Measurements

Diffuse reflectance spectra (DRS) were recorded with a Shimadzu UV-2600 spectrophotometer equipped with an integration sphere. XRD measurements were performed using a Philips PW3020 diffractometer, operating at 40 kV and 40 mA, employing Cu Kα radiation (λ = 1.54056 Å). Quantitative phase analysis was made by the Rietveld refinement method [21], using the "Quanto" software [22]; the average crystallite size was calculated according to the Scherrer equation, as previously described [13]. The BET surface area was determined by N_2 adsorption in a Micromeritics Tristar II 3020 V1.03 apparatus. Current–voltage curves were traced with an Autolab PGSTAT128N potentiostat. IPCE values were measured by employing a home-made installation using a Xenon lamp and interference filters.

3. Results and discussion

3.1. Characterization of powders and films

The three FSP powders studied in the present work were characterized by XRD and BET analysis. Fig. 1 shows XRD diffractograms, which reveal that the powders are produced predominantly in the anatase phase. The percent amounts of anatase and rutile are given in Table 1, together with the size d_A of the nanoparticles and the specific surface area SSA. Nanoparticle size was evaluated from XRD data (anatase (1 0 1) reflection) through the Scherrer equation.

As expected, larger SSA values correspond to smaller nanoparticles. The smallest nanoparticles were obtained in the case of FSPb, *i.e.*, the powder produced by using a 0.45 M TTIP solution in xylene at the smallest flow of 1 mL min^{-1}. Their size was 7 nm and they possessed a very large SSA of 249 m^2 g^{-1}. Slightly larger nanoparticles were obtained by increasing the precursor solution flow, but this was accompanied by a remarkable SSA decrease. When the concentration of TTIP in the burnt solution was increased to 0.80 M, the particles underwent a dramatic increase of size and equally suffered a dramatic decrease of SSA, which became 15 nm and 90 m^2 g^{-1}, respectively. Obviously, in order to keep the particle size small and the SSA large, FSP should be limited to low titanium precursor concentration in the solution fed to the burner and to small solution flow rates [13].

The FSP-made powders were used to make pastes and to be deposited as thin films on FTO electrodes. A representative FESEM image of the calcined films, is shown in Fig. 2. A rough estimation of

Table 1
Synthesis parameters; phase composition (A = anatase, R = rutile) obtained by the Rietveld refinement of XRD data assuming the absence of amorphous phase; anatase crystallite size, d_A, calculated from XRD analysis by applying the Scherrer equation; specific surface area (SSA) obtained by BET isotherms; cluster sizes d_C were obtained from FESEM images of the FSP-made TiO_2 films on FTO electrodes.

Sample	TTIP (M)	Precursor flow (mL min^{-1})	O_2 dispersion (L min^{-1})	A (wt%)	R (wt%)	d_A (nm)	SSA (m^2 g^{-1})	d_C (nm)
FSPa	0.80	4	5	78	22	15	90	50–70
FSPb	0.45	1	5	88	12	7	249	7–15
FSPc	0.45	4	8	73	27	9	161	12–25
P25	-	-	-	70	30	25	45	20–30

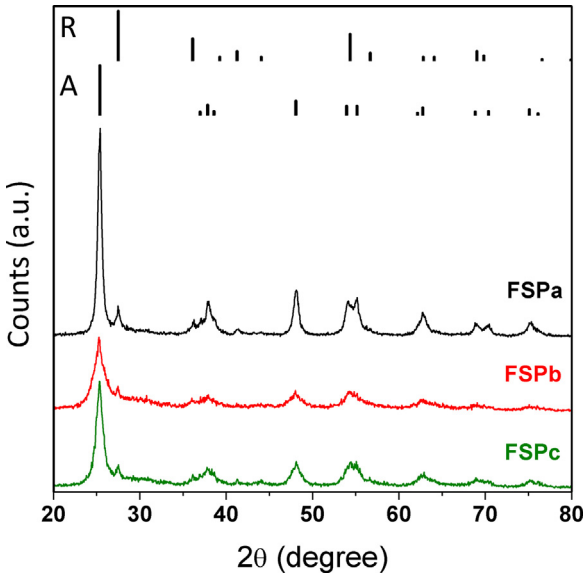

Fig. 1. XRD patterns of powders FSPa, FSPb and FSPc. The peaks positions of the anatase (A) and rutile (R) TiO_2 crystal phases are reported on top.

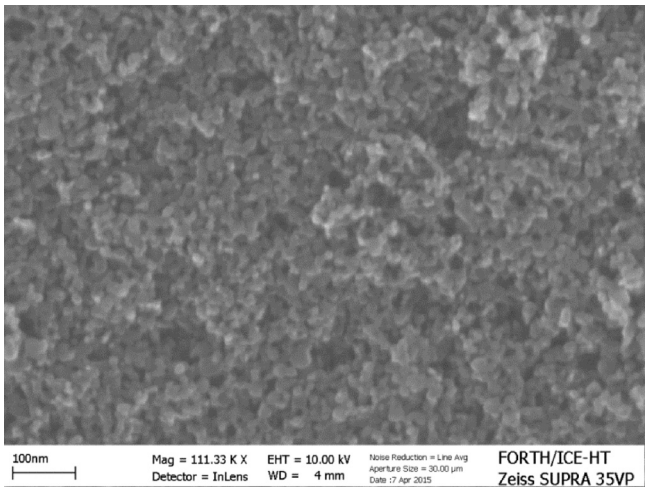

Fig. 2. FESEM image of a film made by depositing a paste of FSPb powder followed by calcination. The scale bar is 100 nm, the particle sizes range between 7 and 15 nm.

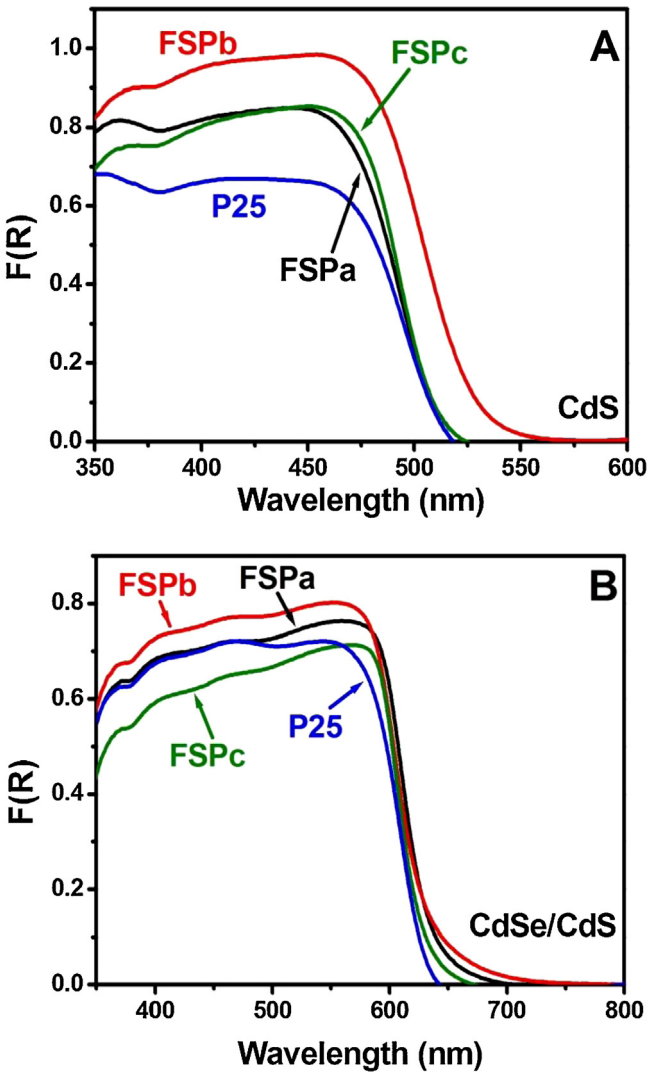

Fig. 3. Diffuse reflectance spectra of (A) CdS/TiO_2/FTO and (B) CdSe/CdS/TiO_2/FTO photoanodes made with the various titania powders. The amount of titania was *ca.* 3 mg cm^{-2} in each film.

the particle size from FESEM images revealed that the particle size in the films follows the same trend as in their powder form, *i.e.*, the smallest particles in the films were obtained starting from the FSPb powder. FESEM images show particle clusters rather than isolated nanoparticles. The corresponding sizes d_C can be found in Table 1. The films made of FSPb powder gave clusters ranging between 7 and 15 nm in size. On the contrary, in the case of FSPa powders, the cluster size ranged between 50 and 70 nm.

The above data show that films with the finest nanoparticle distribution were obtained from FSPb powders, *i.e.*, the material with the smallest nanoparticles and the highest SSA. When such films come in contact with the liquid phase they are expected to create the most efficient interface and the most efficient photoanodes and this should reflect on the electrical characteristics of the cells.

Photoanodes made by the above titania films were sensitized in the visible region by CdS or combined CdS + CdSe quantum dot sensitizers, which were formed on the titania films by precursor adsorption from chemical baths. The films made with the three different FSP powders and with commercial Degussa P25 demonstrated a different CdS loading capacity, that matched their SSA. This is shown by the diffuse reflection spectra of Fig. 3A. Commercial P25 with the smallest SSA (Table 1) gave the lowest CdS light absorbance, while FSPb with the largest SSA gave the highest

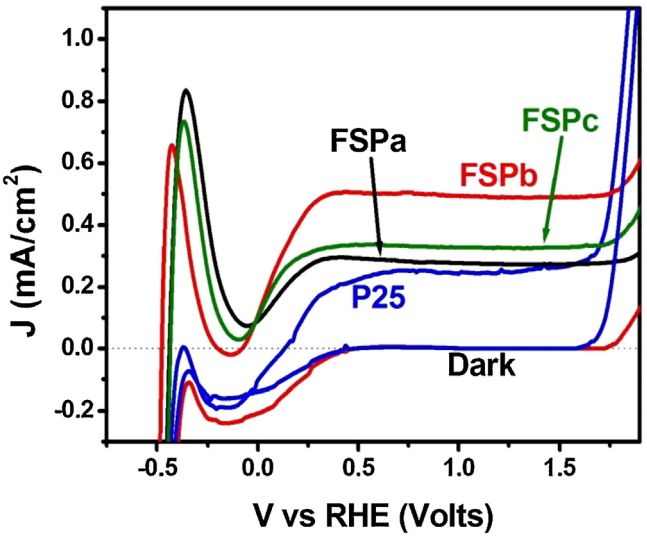

Fig. 4. Current–voltage curves obtained with a photoelectrochemical cell comprising a photoanode made of various titania films. The two "Dark" curves at the bottom correspond to P25 and FSPb. The electrolyte contained only 0.5 M NaOH.

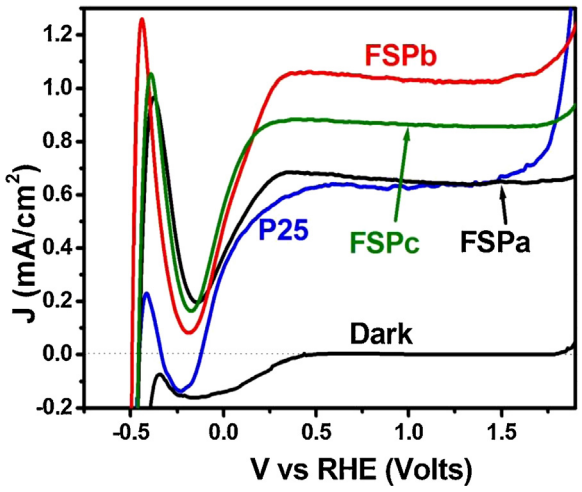

Fig. 5. Current–voltage curves obtained with a photoelectrochemical cell comprising a photoanode made of various titania films. The electrolyte solution contained 0.5 M NaOH + 5% v/v ethanol.

absorbance. Higher CdS loading results in the formation of larger nanoparticles, thus longer wavelength absorption onset. Indeed, in the case of FSPb, CdS absorption threshold was red-shifted by approximately 50 nm.

This clear distinction between the different titania films was practically lost when CdSe was additionally deposited on the electrodes. The amount of chemical-bath deposited CdSe is highly affected by the CdS seeds that precede CdSe deposition. The amount of CdSe deposited in the absence of any CdS seeds was very low or negligible [15]. For this reason, when CdSe was added on top of CdS/TiO_2/FTO, the light absorption differences between the four electrodes were much smaller than in the case of the sole CdS deposition (see Fig. 3b). Nevertheless, FSPb-based films still gave the highest absorbance and the longest absorption threshold.

3.2. Photoelectrochemistry of water oxidation using various titania photoanodes

Titania is the most celebrated photocatalyst and this is for very good reasons. It is easily synthesized and deposited as thin film, it is very stable and it easily oxidizes water, thanks to its highly positive valence band potential (about 3 V *vs* SHE). As seen in Fig. 4, its anodic photocurrent onset appeared at about 0.13 V *vs* RHE. The diagram of Fig. 4 was obtained by using the actual values recorded *vs* a Ag/AgCl reference electrode and by adding 0.98 V (0.2 V + 0.059 × 13.2 V, for pH 13.2). Photocurrent plateau was attained at about 0.5 V *vs* RHE; however, the plateau height depended on the quality and the functionality of the employed film.

The merits associated with the highest SSA FSPb powder are clearly demonstrated by the data of Fig. 4, which show the basic photoelectrochemical parameters of a water splitting reactor. Water is oxidized at the photoanode consuming photogenerated holes while photogenerated electrons move through the external circuit and they reduce water at the cathode electrode. The current flowing is proportional to the amount of hydrogen produced. Monitoring hydrogen production was not considered necessary in the present work. In fact, the recorded photocurrent values may be used as a measure of the photoanode activity, since previous studies have demonstrated that photocurrent density perfectly parallels the rate of hydrogen production by water splitting [23].

Fig. 4 then shows that the recorded plateau value of the current density was about twice as large in the case of FSPb than in P25. By excitation with monochromatic radiation peaking at 380 nm, the IPCE% value was measured for these two photoanodes using the standard formula:

$$\text{IPCE\%} = \frac{1240 \times J_{sc}(\text{mA/cm}^2)}{\lambda(\text{nm}) \times P(\text{mW/cm}^2)} \times 100 \quad (1)$$

where, J is the current density, P is the intensity of the incident radiation and λ is the wavelength. IPCE% was then found 41 and 86% for the P25 and FSPb photoanode, respectively, for an incident UVA radiation intensity equal to 1.9 mW cm^{-2} and for of 1.0 V *vs* RHE bias. The superiority of FSPb is then reflected also on the IPCE values.

The *JV* curves of Fig. 4 contain an intense anodic peak at about −0.4 V *vs* RHE (−1.4 V *vs* Ag/AgCl). This peak corresponds to the adsorption of Na^+ cations of the electrolyte by the titania film at negative potentials, a matter that has been analyzed in a previous publication [24]. It is interesting to note that this peak is particularly intense in the case of FSP-produced titania and it can be, obviously, associated with the high SSA obtained with these materials. This intense peak affects the position of the anodic photocurrent onset, which appears at smaller anodic bias than in the case of P25. The strong anodic current on the right side of each curve is due to water electrolysis. Interestingly, FSP photoanodes need a little higher anodic bias to achieve water electrolytic oxidation than P25 photoanodes. This is clearer by comparing the curves recorded in the dark, also shown in Fig. 4.

3.3. Photoelectrochemical cells acting as ethanol PhotoFuelCells

When ethanol was added to the electrolyte solution, the recorded currents increased, in fact more than doubled, as evidenced by a comparison between the current density plateaus reported for each film in Figs. 4 and 5. This current increase may derive from a more efficient consumption of holes and suppression of electron-hole recombination, but it may also derive from current-doubling effects [25] (and references therein). Current doubling originates from the formation of unstable radicals by ethanol oxidation, followed by electron injection from these radicals into the conduction band of the photocatalyst. The IPCE% values measured in the presence of ethanol were 106 and 179% for the P25 and FSPb photoanode, respectively, for an incident UVA radiation intensity equal to 1.9 mW cm^{-2} and a 1.0 V *vs* RHE applied bias. Thus, IPCE% values above 100% were obtained with both photoanodes and this may be explained only by the presence of current dou-

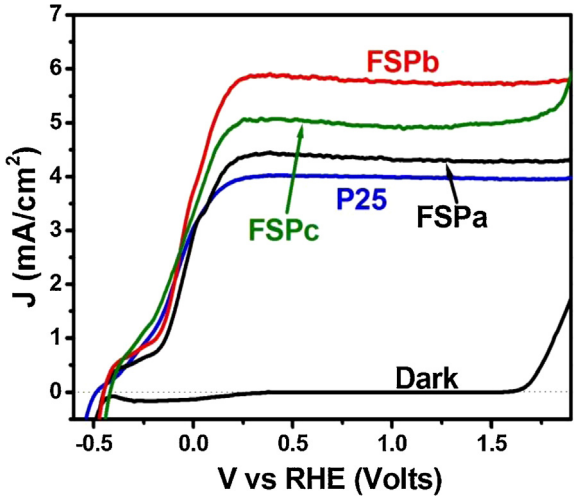

Fig. 6. Current–voltage curves obtained with a photoelectrochemical cell comprising various CdS/TiO_2/FTO photoanodes. The electrolyte contained 0.5 M NaOH + 5% v/v ethanol.

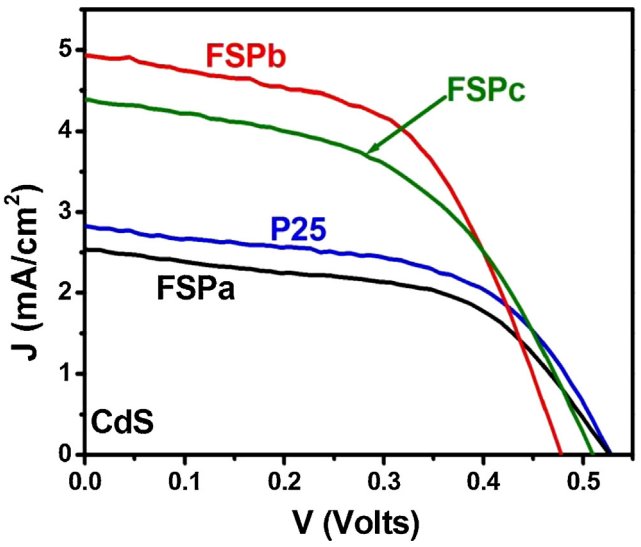

Fig. 7. Current–voltage curves obtained with a quantum dot sensitized solar cell with various CdS/TiO_2/FTO photoanodes and a Cu_2S/brass counter electrode. The polysulfide electrolyte contained 1.0 M Na_2S + 1.0 M S.

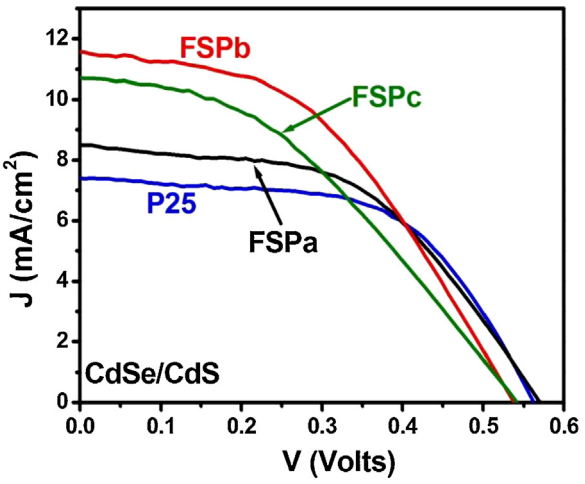

Fig. 8. Current–voltage curves obtained with a quantum dot sensitized solar cell carrying various CdSe/CdS/TiO_2/FTO photoanodes and a Cu_2S/brass counter electrode. The polysulfide electrolyte contained 1.0 M Na_2S + 1.0 M S.

bling effects [25]. It must be underlined at this point that recorded current is stable for a short measuring time range. For a longer time range, the current slowly dropped due to ethanol consumption. This of course depends on ethanol content and on the rate of its consumption.

Fig. 5 shows the presence of the above discussed anodic peak at −0.4 V *vs* RHE also in the presence of ethanol, indicating that the presence of this organic additive did not prevent Na^+ adsorption on the photocatalyst films.

3.4. PhotoFuelCells with sensitized photoanodes

Titania photoanodes can be sensitized by CdS quantum dots and they demonstrate satisfactory stability in the presence of ethanol [26]. This was explained by the fact that the combined CdS/TiO_2 photocatalyst has an oxidative power high enough to produce hydroxyl radicals, which govern ethanol oxidation. On the contrary, CdSe/CdS/TiO_2 or CdSe/TiO_2 combined semiconductors do not have this capacity. For this reason, PhotoFuelCells running with organic fuels are operated only with CdS quantum dot sensitizers, and this has been done also in the present work.

Fig. 6 shows the current–voltage characteristics of such cells. As expected, the current now reached much higher values, thanks to the broader exploitation of the visible spectrum. Once again FSPb was the best titania photocatalyst. The order of efficiency, in terms of current, was the same as those of SSA values and CdS loading (see Fig. 3). Interestingly, the Na^+ adsorption peak at −0.4 V *vs* RHE was now effectively suppressed. This is expected, since CdS deposition on titania prevents further cation adsorption.

The band gap of the combined CdS/TiO_2(FSPb) photocatalyst, as derived from the corresponding absorption spectrum (Fig. 3A), is 2.4 eV. The maximum photocurrent expected for an ideal photoanode with such a band gap is 7.4 mA cm^{-2} [27]. The saturation current reached in the case of the FSPb photoanode was 5.8 mA cm^{-2}. If we take into account the possibility to overpass the above upper limit by current doubling phenomena, we conclude that FSPb photoanode has not reached its maximum capacity. This might be improved by investigating the effects of film thickness and amount of photocatalyst, that have not been presently optimized.

We can thus conclude that in both water and ethanol oxidation FSP-produced titania demonstrated superior properties than commercial P25, with the FSPb powder being the best performing of all.

3.5. Quantum dot sensitized solar cells

The cases examined so far dealt with photoelectrochemical cells, which function by non-regenerative chemical oxidation and reduction reactions at the two electrodes. However, if a redox electrolyte is introduced in the cell, the system may run as a regenerative solar cell. In the presence of metal sulfide quantum dot sensitizers, a polysulfide redox electrolyte is used and this constitutes a unique choice [15,28]. In the present work, we used photoanodes sensitized by either CdS or both CdS and CdSe. The light absorption properties of the two types of photoanode systems are given in Fig. 3. The *JV* characteristics measured with the so obtained cells are given in Figs. 7 and 8.

Since we now deal with regenerative solar cells, plots were traced in a two electrode configuration, as it is common practice with solar cells. The corresponding parameters are given in Tables 2 and 3. FSPb-made photoanode was once more superior to the other photoanodes, in terms of both short-circuit current density J_{sc} and cell efficiency η. The open-circuit voltage V_{oc} was practically the same in all four cases. The fill factor FF was lower in

Table 2
Solar cell parameters extracted from the diagrams of Fig. 7 (CdS loading).[a]

Type of titania	J_{sc} (mA cm^{-2})	V_{oc} (V)	FF	η
P25	2.8	0.52	0.56	0.8
FSPa	2.6	0.52	0.54	0.7
FSPb	4.9	0.48	0.55	1.3
FSPc	4.4	0.51	0.49	1.1

[a] All values of this table are recorded with 1% error.

Table 3
Solar cell parameters extracted from the diagrams of Fig. 8 (CdSe/CdS loading).[a]

Type of titania	J_{sc} (mA cm^{-2})	V_{oc} (V)	FF	η
P25	7.5	0.56	0.57	2.4
FSPa	8.3	0.54	0.49	2.2
FSPb	11.6	0.52	0.46	2.8
FSPc	10.8	0.53	0.40	2.3

[a] All values of this table are recorded with 1% error.

the case of higher current, a tendency usually observed with non-optimized cells. As expected, the overall efficiencies were larger in the presence of CdSe, since a wider range of visible light is absorbed in that case. The differences in efficiency between the four titania types was more pronounced in the case of CdS alone but became less important in the presence of CdSe. The explanation of this can be found in Fig. 3, evidencing that the differences between the various CdS loadings on the photoanodes were large, whereas they were less important in the case of CdSe loading. In other words, the differences between the different types of titania were lost when CdSe was added on top of the CdS sensitized photoanodes. Thus, these differences seem more important in the case of PhotoFuelCells than in the case of CdSe quantum dot sensitized solar cells.

In closing this subsection, it is worth underlining again that the photocurrent data were not optimized in terms of photocatalyst amount in the film, our aim being a comparison between photoanodes with the same photocatalyst load.

4. Conclusions

FSP-made titania nanoparticles may be obtained in powder form with relatively small nanoparticles and large specific surface area. This powder can be used to make pastes to be deposited in thin film and thus prepare electrodes to be used as photoanodes in photoelectrochemical cells for water-splitting and PhotoFuelCell applications. The superiority of FSPb titania was clearly demonstrated with respect to the rest of the here examined samples and, in particular, with respect to commercial P25 titania. The importance of an efficient method for mass production of small size and high SSA titania photocatalyst is here underlined. On the other hand, when titania is loaded with a relatively high amount of sensitizer, namely CdSe, the role of this latter becomes important and decreases the effects related to the differences between the different forms of titania. This was the case of the CdSe/CdS combined sensitizers, which were used in quantum dot sensitized solar cells.

Acknowledgements

This research has been co-financed by the European Union (European Social Fund—ESF) and Greek National Funds through the Operational Program “Education and Lifelong Learning” of the National Strategic Reference Framework (NSRF)—Research Funding Program: Thales. MIS379320. Investing in knowledge society through the European Social Fund. It was also partially supported by the Italian Ministry of University and Research (MIUR) “National Funding for Basic Research” (FIRB RBAP11AYN) project entitled “Oxides at the nanoscale: functionalities and applications”.

References

[1] D. Spasiano, R. Marotta, S. Malato, P. Fernandez-Ibanez, I. Di Somma, Solar photocatalysis: materials, reactors, some commercial and pre-industrialized applications. A comprehensive approach, Appl. Catal. B Environ. 170–171 (2015) 90–123.
[2] A.A. Ismail, D.W. Bahnemann, Photochemical splitting of water for hydrogen production by photocatalysis: a review, Sol. Energy Mater. Sol. Cells 128 (2014) 85–101.
[3] Y. Lan, Y. Lu, Z. Ren, Mini review on photocatalysis of titanium dioxide nanoparticles and their solar applications, Nano Energy 2 (2013) 1031–1045.
[4] A. Kudo, Y. Miseki, Heterogeneous photocatalyst materials for water splitting, Chem. Soc. Rev. 38 (2009) 253–278.
[5] P. Lianos, Production of electricity and hydrogen by photocatalytic degradation of organic wastes in a photochemical cell. The concept of the Photofuelcell: a review of a re-emerging research field, J. Hazard. Mater. 185 (2011) 575–590.
[6] M. Grätzel, Recent advances in sensitized mesoscopic solar cells, Acc. Chem. Res. 42 (2009) 1788–1798.
[7] P. Gao, M. Grätzel, M. Nazeeruddin, Organohalide lead perovskites for photovoltaic applications, Energy Environ. Sci. 7 (2014) 2448–2463.
[8] G.L. Chiarello, M.V. Dozzi, M. Scavini, J.D. Grunwaldt, E. Selli, One step flame-made fluorinated Pt/TiO_2 photocatalysts for hydrogen production, Appl. Catal. B: Environ. 160–161 (2014) 144–151.
[9] G.L. Chiarello, E. Selli, L. Forni, Photocatalytic hydrogen production over flame spray pyrolysis-synthesised TiO_2 and Au/TiO_2, Appl. Catal. B: Environ. 84 (2008) 332–339.
[10] G.L. Chiarello, L. Forni, E. Selli, Photocatalytic hydrogen production by liquid- and gas-phase reforming of CH_3OH over flame-made TiO_2 and Au/TiO_2, Catal. Today 144 (2009) 69–74.
[11] G.L. Chiarello, M.H. Aguirre, E. Selli, Hydrogen production by photocatalytic steam reforming of methanol on noble metal-modified TiO_2, J. Catal. 273 (2010) 182–190.
[12] G.L. Chiarello, D. Ferri, E. Selli, Effect of the CH_3OH/H_2O ratio on the mechanism of the gas-phase photocatalytic reforming of methanol on noble metal-modified TiO_2, J. Catal. 280 (2011) 168–177.
[13] L.G. Bettini, M.V. Dozzi, F. Della Foglia, G.L. Chiarello, E. Selli, C. Lenardi, P. Piseri, P. Milani, Mixed-phase nanocrystaline TiO_2 photocatalysts produced by flame spray pyrolysis, Appl. Catal. B Environ. 178 (2015) 226–232.
[14] R. Michal, S. Sfaelou, P. Lianos, Photocatalysis for renewable energy production using PhotoFuelCells, Molecules 19 (2014) 19732–19750.
[15] S. Sfaelou, A.G. Kontos, P. Falaras, P. Lianos, Micro-Raman, photoluminescence and photocurrent studies on the photostability of quantum dot sensitized photoanodes, J. Photochem. Photobiol. A 275 (2014) 127–133.
[16] P.V. Kamat, Boosting the efficiency of quantum dot sensitized solar cells through modulation of interfacial charge transfer, Acc. Chem. Res. 45 (2012) 1906–1915.
[17] Y.F. Nicolau, Solution deposition of thin solid compound films by a successive ionic-layer adsorption and reaction process, Appl. Surf. Sci. 22–23 (1985) 1061–1074.
[18] S. Sfaelou, L. Syggelou, V. Dracopoulos, A. Travlos, P. Lianos, Effect of the nature of cadmium salts on the effectiveness of CdS SILAR deposition and its consequences of the performance of sensitizes solar cells, J. Phys. Chem. B 118 (2014) 22873–22880.
[19] Q. Shen, D. Arae, T. Toyoda, Photosensitization of nanostructured TiO_2 with CdSe quantum dots: effects of microstructure and electron transport in TiO_2 substrates, J. Photochem. Photobiol. A: Chem. 164 (2004) 75–80.
[20] S. Gorer, G. Hodes, Quantum size effects in the study of chemical solution deposition mechanisms of semiconductor films, J. Phys. Chem. 98 (1994) 5338–5346.
[21] H.M. Rietveld, A profile refinement method for nuclear and magnetic structures, J. Appl. Cryst. 2 (1969) 65–71.
[22] A. Altomare, M.C. Burla, C. Giacovazzo, A. Guagliardi, A.G.G. Moliterni, G. Polidori, R. Rizzi, Quanto: a rietveld program for quantitative phase analysis of polycrystalline mixtures, J. Appl. Crystallogr. 34 (2001) 392–397.
[23] M. Altomare, M. Pozzi, M. Allieta, L.G. Bettini, E. Selli, H_2 and O_2 photocatalytic production on TiO_2 nanotube arrays: effect of the anodization time on structural features and photoactivity, Appl. Catal. B: Environ. 136–137 (2013) 81–88.
[24] L.-C. Pop, S. Sfaelou, P. Lianos, Cation adsorption by mesoporous titania photoanodes and its effect on the current–voltage characteristics of photoelectrochemical cells, Electrochim. Acta 156 (2015) 223–227.
[25] E. Kalamaras, P. Lianos, Current doubling effect revisited: current multiplication in a PhotoFuelCell, J. Electroanal. Chem. 751 (2015) 37–42.
[26] M. Antoniadou, D.I. Kondarides, D.D. Dionysiou, P. Lianos, Quantum dot sensitized titania applicable as photoanode in photoactivated fuel cells, J. Phys. Chem. C 116 (2012) 16901–16909.
[27] Z. Li, W. Luo, M. Zang, J. Feng, Z. Zou, Photoelectrochemical cells for solar hydrogen production: current state of promising photoelectrodes, methods to improve their properties, and outlook, Energy Environ. Sci. 6 (2013) 347–370.
[28] I. Hwang, K. Yong, Counter electrodes for quantum-dot-sensitized solar cells, ChemElectroChem 2 (2015) 634–653.